

Synthesis and characterization of nanocrystalline fluorinated hydroxyapatite powder by a modified wet-chemical process

Hossein Eslami, Mehran Solati-Hashjin and Mohammadreza Tahriri*

Amirkabir University of Technology, Faculty of Biomedical Engineering, Biomaterial Group, P. O. Box: 15875-4413 Tehran, Iran

Fluorinated hydroxyapatite (FHA; fluorhydroxyapatite) powder was synthesized through a pH-cycling method by varying the sodium fluoride [NaF] concentration in a hydroxyapatite suspension as a modified wet-chemical process. The powder sample was characterized by the commonly used bulk techniques of scanning electron microscopy (SEM), Fourier transform infrared spectroscopy (FTIR), x-ray diffraction (XRD), F-selective electrode, atomic absorption spectroscopy (AAS) and EDTA titration analyses. SEM was used to estimate the particles size of the powder and observe the morphology and agglomeration state of the powder. The functional groups presented in the synthesized powder were ascertained by FTIR investigations. AAS and EDTA titration techniques were employed for calculation of the Ca/P molar ratio. F-selective electrode analysis also was used to measure the fluorine (F) content in the crystalline network of the synthesized powder. Finally, the FHA and other phases according to processing parameters were observed by XRD analysis.

Key words: Synthesis, fluorhydroxyapatite, hydroxyapatite, nanocrystalline, fluorine.

Introduction

Synthetic hydroxyapatite (HA; $\text{Ca}_{10}(\text{PO}_4)_6(\text{OH})_2$) has been extensively investigated as a bone substitute material due to its similar chemical composition to that of bone, its direct bone bonding ability, and its commercial availability. However, synthetic HA presents poor thermal stability as indicated by the decomposition into other phases such as tricalcium phosphate (TCP; $\text{Ca}_3(\text{PO}_4)_2$) at sintering temperatures higher than 900 °C. This phase impurity often results in undesirable fast dissolution rates in vivo. The lack of commercially efficient techniques in processing pure HA ceramics to full densification without decomposition has somewhat restricted the wider applications of HA ceramics. In contrast, it is expected that fluorapatite ($\text{Ca}_5(\text{PO}_4)_3\text{F}$) or fluorhydroxyapatite might have superior mechanical properties when sintered at high temperatures because of their higher thermal stability than HA [1].

Fluorinated hydroxyapatite [$\text{Ca}_{10}(\text{PO}_4)_6(\text{OH})_{2-2x}\text{F}_{2x}$ ($0 \leq x \leq 1$)], where F partially replaces OH in hydroxyapatite, is potentially a very interesting biomaterial. It was suggested that fluoride-substituted hydroxyapatite has a better thermal and chemical stabilities than hydroxyapatite [2]. This phenomenon could be explained by considering the crystal structure of HA. The hydrogen (H^+) ions (the smallest spheres in the structure) of HA were arranged in the atomic interstices neighboring the oxygen ions (O_2^-), forming OH^- groups and were oriented

randomly, which conferred a certain degree of disorder to the crystal structure of HA. Once the OH^- groups were partially substituted by the F^- ions, the existing hydrogen ions of the OH^- groups were bound to the nearby F^- ions because of the higher affinity of the F^- ions with respect to the oxygen ions, producing a quite well-ordered apatite structure, which caused an increase of the thermal and chemical stabilities of the HA matrix. Therefore, when a certain amount of F^- ions substituted the OH^- groups in the HA matrix, a certain level of chemical and thermal stability of the FHA ceramics was achieved. Theoretically, a F^- ion concentration of 50% in the FHA should be enough to remove the disorder of the crystal structure of HA and hence stabilize the structure F due to the alternating arrangement of the F^- ions between each pair of OH^- groups. However, by considering the random substitution of OH^- ions with F^- ions in the OH^- positions, the F^- ion concentration required to stabilize the structure was necessarily higher than 50% [1]. Thus, FHA exhibits a very attractive combination of stability and biocompatibility [2]. However, it has been reported that if all of the OH groups in HA are replaced by F to form fluorapatite (FA), the resulting material is not osteo-conductive [3]. Moreover, the high F content might lead to severe adverse effects such as osteomalacia [1]. As a result, various methods have been developed in an attempt to tailor the fluorine content of FHA to achieve the best biological properties. FHA can be either prepared using a solid-state reaction or a wet-chemical process, but the later is used more commonly. There are several methods of synthesizing fluorinated hydroxyapatite with varied fluorine contents, such as, by sol-gel [4] a solid state reaction [5], and pyrolysis methods [6]. The pH-cycling method as the modified wet chemical

*Corresponding author:
Tel : +98(912)2388573
Fax: +98(21)66468186
E-mail: m-tahriri@aut.ac.ir

process was first introduced by Ramsey et al [7] to avoid a high temperature operation and the use of volatilized alcohol (fluorine containing reagent). FHAs formed by these different approaches have been characterized using X-ray diffraction (XRD), Fourier transform infra-red spectroscopy (FTIR) and Scanning electron microscopy (SEM) [8, 9-13]. In this manner, Okazaki et al [8] demonstrated that a laminated structure is formed in micro sized FHA precipitates produced via a multi-step fluorine supply process.

In this research, we are reporting synthesis of nanocrystalline fluorinated hydroxyapatite powder via a pH-cycling method as a modified wet-chemical process, and the resulting powder was characterized by commonly used bulk techniques.

Materials and Methods

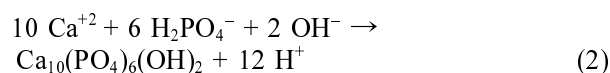
Powder preparation

Synthesis of HA

The flowchart for the synthesis of the hydroxyapatite is illustrated in Fig. 1.

0.09 M diammonium hydrogen phosphate solution $[(\text{NH}_4)_2\text{HPO}_4]$, %99, Merck company Inc.] and 0.15 M calcium nitrate 4-hydrate solution $[\text{Ca}(\text{NO}_3)_2 \cdot 4\text{H}_2\text{O}]$, %98, Merck PROLABO] were prepared and the pH of both solutions was brought to about 11 by adding 1 M

sodium hydroxide solution [NaOH, %99, Merck company Inc.]. The phosphate solution was added drop-wise into the calcium nitrate solution, resulting in the precipitation of HA. The precipitation of HA can be described by reactions (1) and /or (2) [14]:



The precipitate was aged for 22 hours at room temperature on a magnetic stirrer (750 rpm). In the next step the precipitated HA was centrifuged and then washed by de-ionized water. The processes of centrifuging and washing were carried out three times. The resulting powder was dried in a freeze-drier system (Alpha 1-2 LD, Germany) for 10 hours. Lastly, the dried powder was calcined in an electrical box furnace at 900 °C for 1 hour after heating at the rate of 5°K/minute in air.

Synthesis of fluorinated hydroxyapatite (FHA)

The flowchart for the synthesis of the fluorinated hydroxyapatite is illustrated in Fig. 2.

5 gr of HA prepared by the above method was suspended in 500 ml of 0.02 M sodium fluoride [NaF, %98.5, Merck Company Inc.] solution. This system was

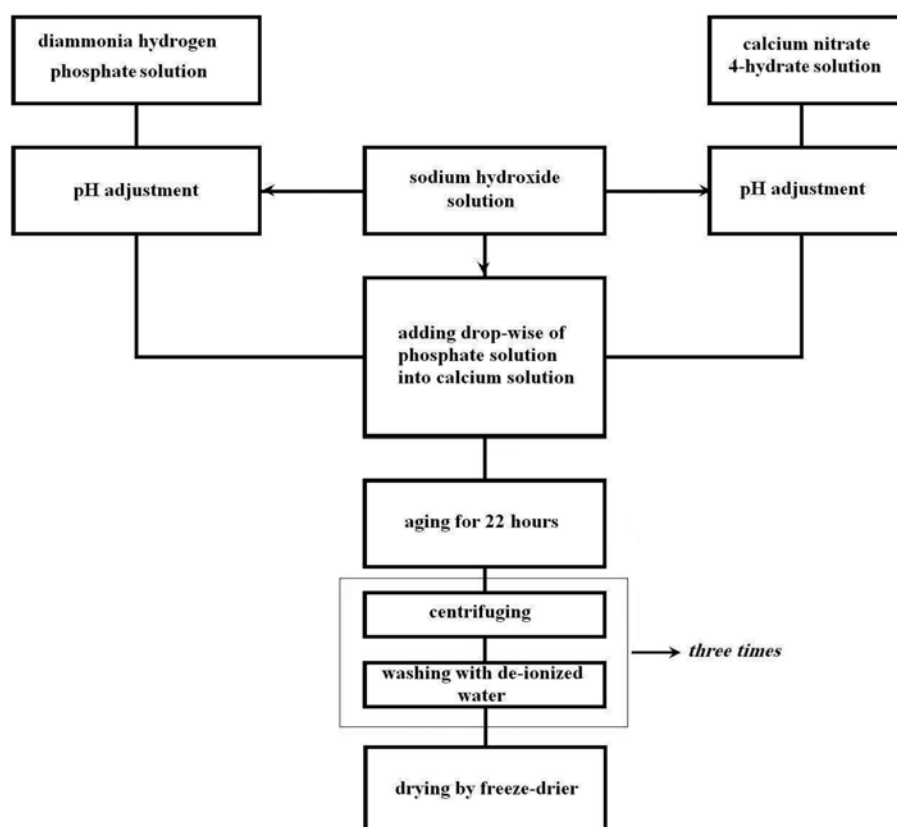


Fig. 1. flowchart for the synthesis of the hydroxyapatite powder.

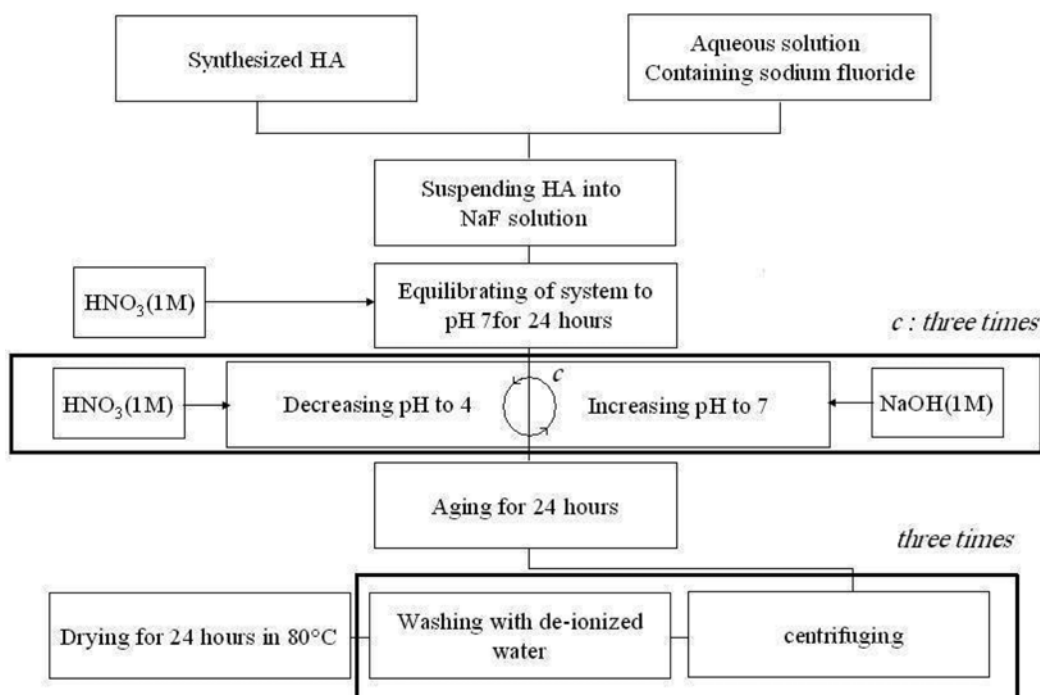
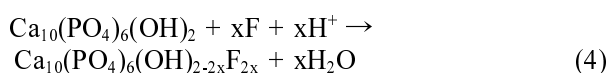
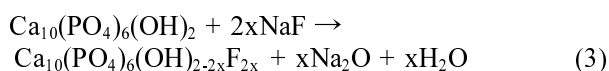


Fig. 2. flowchart for the synthesis of the fluorinated hydroxyapatite powder.

equilibrated to pH 7 for 24 hours. The pH of the solution was decreased to 4 by slowly adding 1 M nitric acid [HNO_3 , %68, Merck Company Inc.]. After 30 minutes, the pH of the solution was brought back to 7 by the addition of 1 M sodium hydroxide (NaOH). The reaction of the FHA synthesis can be expressed by the reactions (3) and /or (4) [2]:



The cycle of pH fluctuation was repeated three times. The solution was centrifuged and then washed with de-ionized water. It is notable that, the processes of centrifuging and washing were carried out three times. The wet powders were dried in an oven at 80 °C for 24 hours. The resulting FHA powder was manually milled by an agate mortar and finally the FHA was calcined in an electrical box furnace at 900 °C for 1 hour after heating up at a rate of 5 °C/min in air.

Powder characterization

X-ray diffraction

The resulting powder was analyzed by X-ray diffraction (XRD) with a Siemens-Brucker D5000 diffractometer. This instrument works with voltage and current settings of 40 kV and 40 mA respectively and uses $\text{Cu-K}\alpha$ radiation (1.540600 Å). For qualitative analysis, XRD diagrams were recorded in the interval $4^\circ \leq 2\theta \leq 70^\circ$ at a scan speed of 2°/minute giving a step size 0.02° and the step time 1 s.

Fourier infra-red spectroscopy

The powder sample was examined by transform Fourier infra-red spectroscopy with a Bomem MB 100 spectrometer. For IR analysis, first 1 mg of the powder sample was carefully mixed with 300 mg of KBr (infrared grade) and palletized under vacuum. Then the pellet was analyzed in the range of 400 to 4000 cm^{-1} at a scan speed of 23 scan/minute with 4 cm^{-1} resolution.

AAS and EDTA titration techniques

In order to calculate the Ca/P molar ratio of the precipitated powder, the content of Ca and P were chemically analyzed by quantitative chemical analysis via an EDTA titration technique and atomic absorption spectroscopy (AAS) with a Shimadzu UV-31005 instrument.

F-selective electrode

Fluorine concentration measurements were conducted using a F-selective electrode in citrate/ hydrochloride acid (TISAB) buffer [5]. 10 mg of the powder sample was dissolved in 0.2 M HCl (20 mg) to which was added 10 mg water and 0.2 M trisodium citrate (40 mg). Standard solution made from NaF was used to calibrate the measurements in the same buffer solution.

Scanning electron microscopy

The powder sample was coated with a thin layer of Gold (Au) by sputtering (EMITECH K450X, England) and then the microstructure of the powder sample was observed in a scanning electron microscope (SEM; Tescan Vega 2XMU) that operated at an acceleration voltage of 15 kV.

Results and Discussion

XRD analysis

Characterization of the FHA was done with XRD. The XRD analysis was performed using the X-ray diffractometer. The straight base line and the sharp peaks of the diffractogram in Fig. 3 confirm that the product is well crystallized. The XRD pattern indicated that approximately pure apatite was formed in this sample, and traces of other calcium phosphate impurities were not detected by this technique. The main HA and FHA phases are difficult to distinguish by X-ray diffraction. Furthermore, some low level impurities may not be detected by XRD, especially if their pattern is overlapped by a stronger pattern. The β -TCP phase in the FHA sample was not observed, indicating its thermal stability [15]. It is notable that in a related figure, a secondary phase CaO (calcium oxide) was observed.

The intensity of the (200) lattice plane of CaO on the XRD pattern of FHA powder was used as a direct indicator of its purity as in the Afshar et al. [16] research. The ratio of the peak intensities on the XRD pattern of CaO/

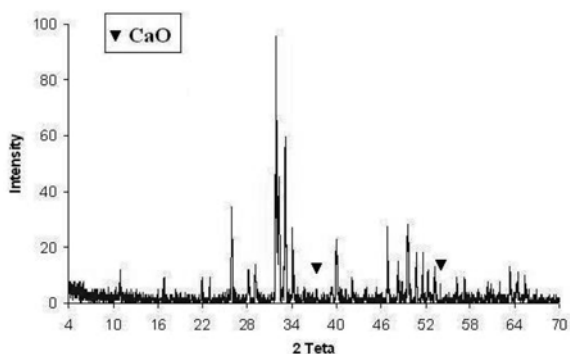


Fig. 3. XRD pattern of the synthesized FHA.

FHA ($I_{(200)\text{CaO}}/I_{(002)\text{FHA}}$), was calculated. The ratio of ($I_{(200)\text{CaO}}/I_{(002)\text{FHA}}$) in the sample was 0.17. It is notable that, the CaO presence does not grant FHA smaller biocompatibility [17]. The control of synthesis parameters commands the development of FHA purity and other phases content in bioceramics [17].

The average crystallite size of the synthesized powder was estimated using the simple Scherrer equation. It can be observed that the value of average crystallite size calculated from the reflection of the planes: (002), (310) and (222) was about 34.5 nm.

FTIR analysis

Figure 4. shows the FT-IR spectrum of FHA powders.

The characteristic bands (listed in table 1) exhibited in the sample spectrum assigned here: (a) the bands at 1042.31 cm^{-1} and 1094.13 cm^{-1} arise from $\nu_3\text{ PO}_4$, the bands at 601.753 cm^{-1} and 576.048 cm^{-1} arise from $\nu_4\text{ PO}_4$, the bands at 962.426 cm^{-1} arises from $\nu_1\text{ PO}_4$ and the bands at 441.458 cm^{-1} and 473.572 cm^{-1} arise from $\nu_2\text{ PO}_4$ (b) the bands at 744.718 cm^{-1} and about 1500 cm^{-1} arise from CO_3 (c) The bands at 3536.9 cm^{-1} arises from OH...F bond.

The FT-IR analysis showed all the typical absorption characteristics of fluorhydroxyapatite. In addition, some carbonate content also was seen (CO_3^{2-} peak around

Table 1. Infrared assigned for the synthesized FHA

Assignment	Infrared frequency (cm^{-1})
OH...F bond	3536.9
$\nu_3\text{ PO}_4^{3-}$ stretch	1042.31, 1094.13
$\nu_1\text{ PO}_4^{3-}$ stretch	962.426
CO_3^{2-}	744.718, ~ 1500
$\nu_4\text{ PO}_4^{3-}$ bend	576.048, 601.753
$\nu_2\text{ PO}_4^{3-}$ bend	441.458, 473.572

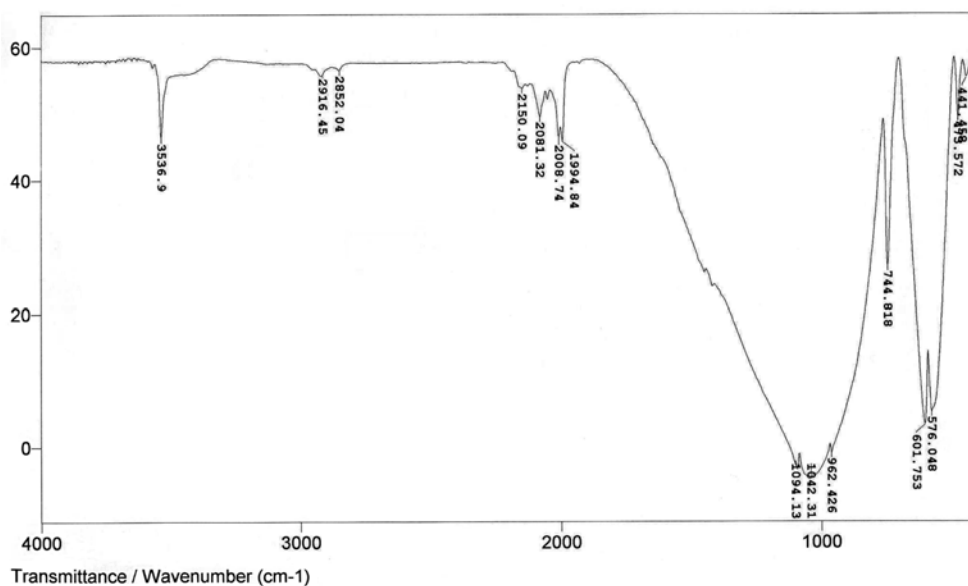


Fig. 4. FT-IR spectrum of the synthesized FHA.

1500 cm^{-1} and 744.718 cm^{-1}), which is an indication of the presence of carbonate apatite. This might have originated through the absorption of carbon dioxide from the atmosphere [18, 19]. Finally, the 3536.9 cm^{-1} band due to OH...F bond was observed in this figure that demonstrated some of the OH groups in the crystalline network of HA were replaced by F.

Therefore according to this explanation, it is obvious that the synthesized powder is certainly fluorhydroxyapatite (FHA).

Elemental analysis

The result of measurement of elemental composition (Ca and P content) and Ca/P molar ratio are summarized in table 2.

The bulk Ca/P molar ratio was determined as 1.71. The measured Ca/P ratio for this synthesized powder was higher than the stoichiometric ratio (1.667) expected for a pure HA (or FHA) phase that can arise for two reasons: (a) the local presence of carbonate apatite in which the Ca/P ratio can be as high as 3.33 [19]. or (b) the presence of impurities such as CaO.

According to the XRD pattern that showed the existence of small amounts of CaO phase, the second explanation is much more reasonable.

F-selective electrode analysis

F-selective electrode analysis also was used to measure the fluorine (F) content in the crystalline network of the synthesized powder. The fluorine (F) content was determined as 2.51%. The F/Ca ratio is summarized in table 3.

It is notable that, Equation (4) explains the calculation of X in the $\text{Ca}_{10}(\text{PO}_4)_6(\text{OH})_{2-2x}\text{F}_{2x}$ formula:

$$\frac{2.51}{38X} = \frac{100}{1004 + 30X} \rightarrow X = 0.65 \quad (5)$$

With respect to the calculated amount of X, the formula of the synthesized fluorhydroxyapatite in this research is $\text{Ca}_{10}(\text{PO}_4)_6(\text{OH})_{0.7}\text{F}_{1.3}$. Therefore, the efficiency of F- incorporation into the HA was calculated as 65%.

SEM observations

SEM was used to investigate the morphology and particle size of the synthesized powder. Typical SEM

Table 2. Ca and P content in the synthesized FHA powder and Ca/P molar ratio

Element	Measured content (wt%)	(Ca/P) molar ratio
Ca	38.63	1.71
P	17.48	

Table 3. F and Ca content in the synthesized FHA powder and F/Ca molar ratio

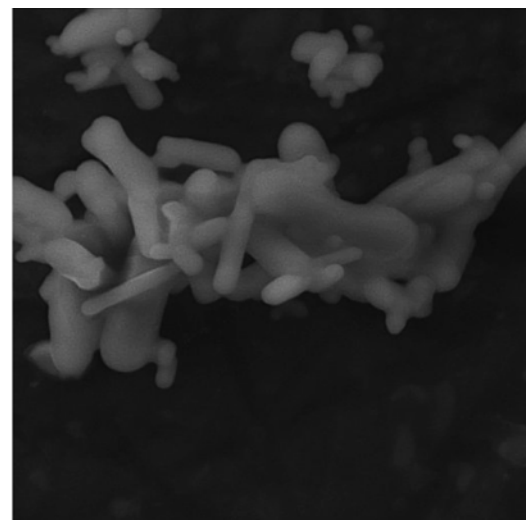
Element	Measured content (wt%)	(F/Ca) molar ratio
F	2.51	0.13
Ca	38.63	

micrographs of synthesized powder at different magnifications are shown in Fig. 5.

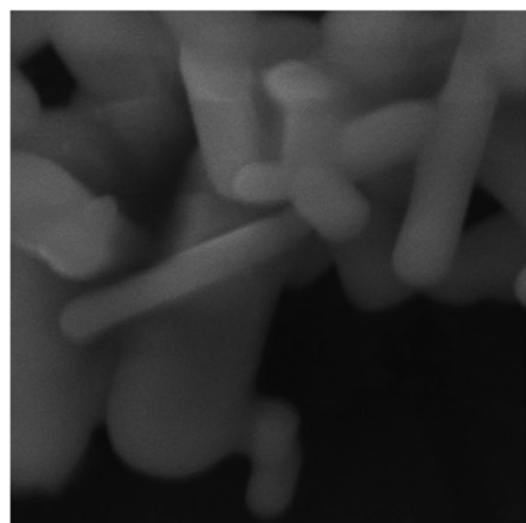
The microstructure of the fluorhydroxyapatite particles was observed as almost rod-like with different aspect ratios. As you can see in this figure, the length and diameter of some rod-like fluorhydroxyapatite has been determined.

Reaction mechanism

When the HA powder was suspended in the NaF solution, FHA was formed through ion-exchange between F and OH [20, 21]. It was suggested that when the pH of the fluoride solution decreased from 7 to 4, more HA dissolved into the solution (in fact, the Ca^{2+} ions dissociates from the surface of hydroxyapatite particles)



(a)



(b)

Fig. 5. SEM micrographs of the synthesized FHA powder at (a) low and (b) high magnification

and then Ca^{+2} ions rapidly reacted with F ions, and formed calcium fluoride (CaF_2). The CaF_2 then reacted with the other ions in the solution and formed precalcination fluorhydroxyapatite as the pH increased to 7.

It is notable that, during the calcination process, the hydroxyapatite containing fluorine (FHA) turned become homogenous [5]. The reason for this phenomenon is interdiffusion of F and OH^- ions [2].

Conclusions

In conclusion, fluorhydroxyapatite was synthesized through a pH-cycling method by varying sodium fluoride (NaF) concentration in hydroxyapatite suspension as a modified wet-chemical process. Synthesized fluorhydroxyapatite powder has been characterized on a macroscopic level by XRD, FTIR and chemical analysis (AAS, EDTA titration technique and F-selective electrode), while SEM has provided detailed information at the microscopic (individual grain) level. The XRD analysis showed that the fluorhydroxyapatite sample prepared was nearly pure fluorhydroxyapatite. Only low levels of specific impurities (such as CaO) were detected and it was also demonstrated that the crystallites of FHA were nanosize. FTIR investigations also showed all the typical absorption characteristics of fluorhydroxyapatite. Chemical analyses (for example AAS and EDTA titration and F-selective electrode analysis) were used for the determination of Ca/P molar ratio and calculation of the replaced fluorine content in the crystalline network of hydroxyapatite. The bulk Ca/P ratio was determined as 1.71 which showed the measured Ca/P ratio for the synthesized powder was higher than stoichiometric ratio (1.667) which is expected for a pure HA (or FHA) phase. Also According to the F-selective electrode analysis result and calculations performed, the achieved formula of the synthesized fluorhydroxyapatite in this research is $\text{Ca}_{10}(\text{PO}_4)_6(\text{OH})_{0.7}\text{F}_{1.3}$. Finally, the SEM technique ascertained that the particles of prepared powder were rod-like.

References

1. Y. Chen and X. Miao, *Biomaterials* 26 (2005) 1205-1210.
2. H. Qu, A.L. Vasiliev, M. Aindow and M. Wei, *J. Mater. Sci. Mater. Med.* 16 (2005) 447-453.
3. L.M. Rodríguez-Lorenzo, J.N. Hart and K.A. Gross, *Biomaterials* 24 (2001) 3777-3785.
4. G.E. Stan and J.M.F. Ferreira, *Digest Journal of Nanomaterials and Biostructures* 1 (2006) 37-42.
5. H. Qu and M. Wei, *Mater. Sci. Mater. Med.* 16 (2005) 129-133.
6. U. Partenfelder, A. Engel and C. Russel, *J. Mater. Sci. Mater. Med.* 4 (1993) 292-295.
7. A.C. Ramsey, E.J. Duff, L. Paterson and J.L. Stuart, *Caries. Res.* 7 (1973) 231-244.
8. M. Okazaki, Y. Miake, H. Tohda, T. Yanasisawa, T. Matsumoto and J. Takahashi, *Biomaterials* 20 (1999) 1421-1426.
9. I. Nikèeviaea, V. Jokanovia, M. Mitria, Z. Nedia, D. Makovec and D. Uskokovia, *J. Solid State Chemistry* 177 (2004) 2565-2574.
10. M. Okazaki, H. Tohda, T. Yanasisawa, M. Taira and J. Takahashi, *Biomaterials* 19 (1998) 919-923.
11. G. Penel, G. Leroy, C. Rey, B. Sombret, J.P. Huvenne and E. Bres, *J. Mater. Sci. Mater. Med.* 8 (1997) 271.
12. K. Sakamoto, S. Yamaguchi, J. Ichihara, M. Okazaki, Y. Tsunawaki and J.C. Elliott, *Journal of the ceramic society of Japan* 112 (2004) 6-12.
13. M. Okazaki and J. Takahashi, *Biomaterials* 16 (1995) 703-707.
14. J.G. Morales, J.T. Burgues, T. Boix, J. Fraile and R.R. Clemente, *Cryst. Res. Technol.* 36 (2001) 15-26.
15. N. Rameshbabu, T.S.S. Kumar and K.P. Rao, *Bull. Mater. Sci.* 29 (2006) 611-615.
16. A. Afshar, M. Ghorbani, N. Ehsani, M.R. Saeri and C.C. Sorrell, *Materials & Design* 24 (2003) 197-202.
17. M.H. Santos, M. de Oliveira, L.P. de Freitas Souza, H.S. Mansur and W.L. Vasconcelos, *Mater. Res.* 7 (2004) 625-630.
18. M. Komath and H.K. Varma, *Bull. Mater. Sci.* 26 (2003) 415-422.
19. M. Wei, J.H. Evans, T. Bostrom and L. Grondahl, *J. Mater. Sci. Mater. Med.* 14 (2003) 311.
20. L.M. Rodríguez-Lorenzo and K.A. Gross, *J. Mater. Sci. Mater. Med.* 14 (2003) 939-943.
21. S. Chander, C.C. Chiao and D.W. Fuerstenau, *J. Dent. Res.* 61 (1982) 403-407.